PCCP

Accepted Manuscript

This is an *Accepted Manuscript*, which has been through the Royal Society of Chemistry peer review process and has been accepted for publication.

Accepted Manuscripts are published online shortly after acceptance, before technical editing, formatting and proof reading. Using this free service, authors can make their results available to the community, in citable form, before we publish the edited article. We will replace this *Accepted Manuscript* with the edited and formatted *Advance Article* as soon as it is available.

You can find more information about *Accepted Manuscripts* in the **Information for Authors**.

Please note that technical editing may introduce minor changes to the text and/or graphics, which may alter content. The journal's standard **Terms & Conditions** and the **Ethical guidelines** still apply. In no event shall the Royal Society of Chemistry be held responsible for any errors or omissions in this *Accepted Manuscript* or any consequences arising from the use of any information it contains.

Journal Name

ARTICLE

Extremely strong organic-metal oxide electronic coupling caused by nucleophilic addition reaction

Jun-ichi Fujisawa*[ab] and Minoru Hanaya[a]

Electronic interplay between organic materials and inorganic semiconductors plays an important role in various electronic and optoelectronic functions, and also provides new functions such as optical interfacial charge-transfer (ICT) transitions having the following features. ICT transitions enable to capture lower-energy photons than HOMO-LUMO gaps or band gaps, and allow for one-step charge separation without energy loss. The hybrid material generated by the nucleophilic addition reaction between TiO$_2$ and TCNQ exclusively shows strong ICT transitions. In this paper, we report that strong organic-metal oxide electronic coupling is caused by the nucleophilic addition reaction, which enhances the ICT transitions. The electronic coupling between TiO$_2$ and TCNQ occurs according to the two-step mechanism. First, the lowest unoccupied molecular orbital (LUMO($\pi*$)) of TCNQ is elevated by the nucleophilic attack of a deprotonated hydroxy group on TiO$_2$ to TCNQ and the electronic distribution is moved toward TiO$_2$. By the elevation and redistribution, the LUMO ($\pi*$) strongly interacts with the $d(t_{2g})$ orbitals of a surface Ti atom. From the avoided-crossing behavior with a large splitting energy of ca. 0.95 eV, the coupling energy was estimated to be as much as 0.5 eV in the mono-Ti model complex. This strong d-$\pi*$ electronic coupling leads to strong coupling between the complete ICT excited states and partial ICT excited state with a large splitting energy of ca. 0.92 eV, which considerably increases the ICT-transition probabilities. This work clarified the mechanisms of the strong organic-inorganic electronic coupling and the enhancement of the ICT absorption in the TiO$_2$-TCNQ hybrid material.

Introduction

Electronic interplay between organic materials and inorganic semiconductors plays an important role in electronic and optoelectronic functions such as photovoltaic conversions[1,2] and electrochemical and photocatalytic reactions[3] in organic-inorganic hybrid systems. Especially, strong electronic coupling at organic-inorganic interfaces not only allows barrier-less fast interfacial electron transfers, but also provides new functions such as optical interfacial charge-transfer (ICT) transitions. ICT transitions have the following exclusive features. ICT transitions enable to capture lower-energy photons than HOMO-LUMO gaps of organic materials or band gaps of inorganic semiconductors. In addition, ICT transitions allow for direct charge separation without energy loss. Because of the potential features, ICT transitions have been expected to be applied to solar energy conversions such as photovoltaic conversion. So far, ICT transitions at organic-inorganic interfaces have been reported in two nanomaterials. One is TiO$_2$
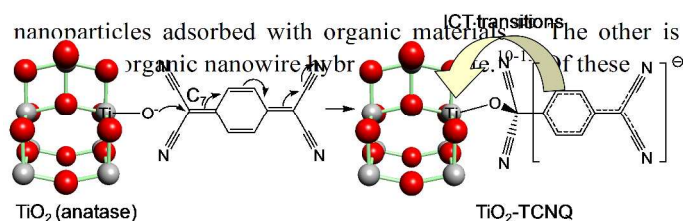

Fig. 1. Nucleophilic addition reaction of an anionic oxygen atom on TiO$_2$ to TCNQ. Gray: titanium and red: oxygen atom.

nanoparticles adsorbed with organic materials. The other is organic nanowire hybrid... i.e. ... of these materials, organic-inorganic hybrid materials generated from titanium dioxide (TiO$_2$) nanoparticles and bis(dicyanomethylene) compounds (TCNX) such as 7,7,8,8-tetracyanoquinodimethane (TCNQ) exclusively show strong organic-to-inorganic ICT transitions.[7,14-16] As shown in Fig. 1, the TiO$_2$-TCNX hybrid materials are produced by nucleophilic addition of a deprotonated surface hydroxy group to TCNX, generating negatively-charge σ-type complexes on TiO$_2$. The

hybrid materials exhibit deep color due to the ICT transitions in the visible-to-near IR region, as shown in Fig. 2(a). Recent theoretical analyses based on density functional theory (DFT)
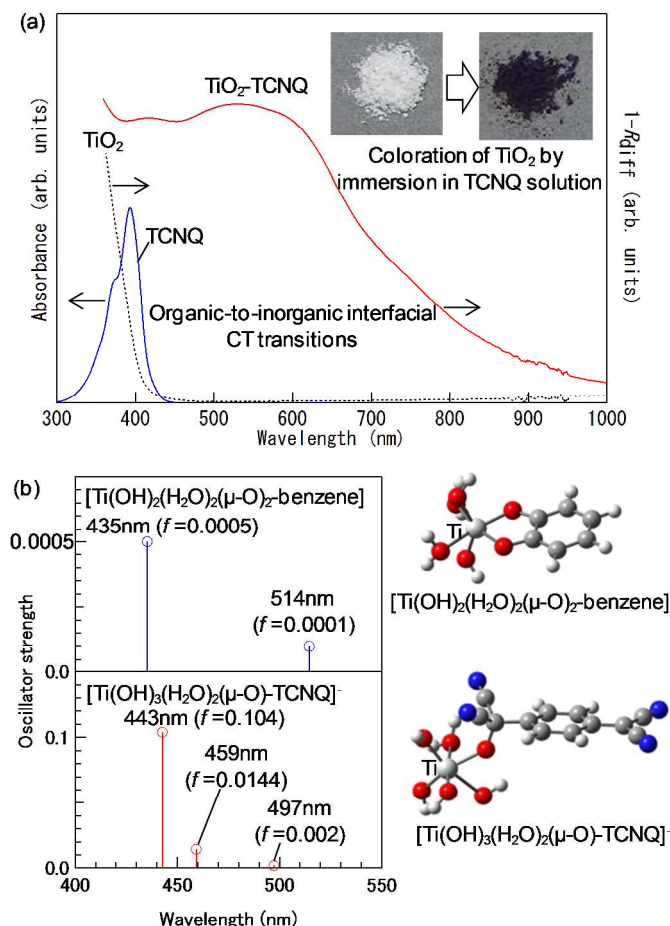

Fig. 2. (a) Diffuse reflectance spectra and photographs of TiO_2 nanoparticles before (black dashed curve) and after (red curve) immersion in TCNQ solution (solvent: acetonitrile) together with the absorption spectrum of TCNQ (blue curve) and (b) calculated electronic excitation spectra of the model compounds, $[Ti(OH)_2(H_2O)_2(\mu\text{-}O)_2\text{-benzene}]$ (blue) and $[Ti(OH)_3(H_2O)_2(\mu\text{-}O)\text{-TCNQ}]^-$ (red) for TiO_2-catechol and TiO_2-TCNQ surface complexes, respectively. The experimental diffuse reflectance and absorption spectra were reported in Refs. 7 and 14. Large gray: titanium, small gray: carbon, white: hydrogen, and red: oxygen atom.

revealed that the ICT-transition probabilities in the TiO_2-TCNX surface complexes are more than one order of magnitude higher than those in the other TiO_2-organic complexes such as TiO_2-catechol[4], as shown in Fig. 2(b).[17] This result suggests that unprecedented strong organic-semiconductor electronic coupling is caused by the nucleophilic addition reaction as compared to conventional chemical adsorptions[1,2]. However, the questions of how the nucleophilic addition reaction causes such strong organic-semiconductor coupling and of how the ICT transition probabilities are enhanced still remain to be clarified. In this paper, we report the mechanisms of strong electronic couplings between TiO_2 and TCNQ and the enhancement of the ICT transitions. For this purpose, the ground state and occupied orbitals of the TiO_2-TCNQ complex were studied in the previous work.[16] However, strong coupling between TiO_2 and TCNQ was not found. In this work, we

extended our attention to the excited states and unoccupied orbitals and found strong coupling between TiO_2 and TCNQ.
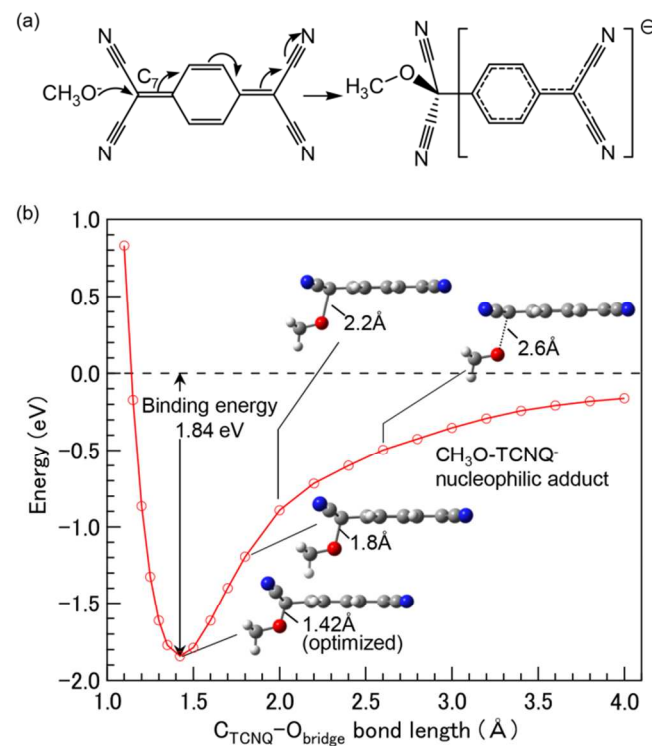

Fig. 3. (a) Nucleophilic addition reaction between a methoxy anion and TCNQ and (b) calculated potential curve of CH_3O-TCNQ⁻ as a function of the C_{TCNQ}-O_{bridge} bond length. Gray: carbon, white: hydrogen, and red: oxygen atom.

In the DFT calculations, we employed mono-Ti model compounds. For TiO_2 nanoparticle-based models[14,16], dependences on crystal faces and effects of adsorption of hydroxy groups and water molecules should be taken into account. In addition, surface structures of TiO_2 nanoparticles have not been understood well yet. For these reasons, the use of mono-Ti model compounds would be appropriate as a first step for understanding of those mechanisms, focusing on the local Ti-O-TCNQ⁻ structure.

Computational details

Structures, energies and electronic distributions of molecular orbitals of mono-Ti model compounds were calculated by DFT[18] with the widely employed B3LYP functional[19,20] and 6-31G+(d,p) basis set[21,22]. Electronic excitation spectra were computed by time-dependent DFT (TD-DFT)[23] at the same level of theory (B3LYP, 6-31G+(d,p)), since the B3LYP functional has been reported to well reproduce the ICT-transition properties.[7,14,17] In all the calculations, solvation effects of acetonitrile used in the reported experiments[7,14] were taken into account with the conductor-like polarizable continuum model (CPCM)[24,25], since

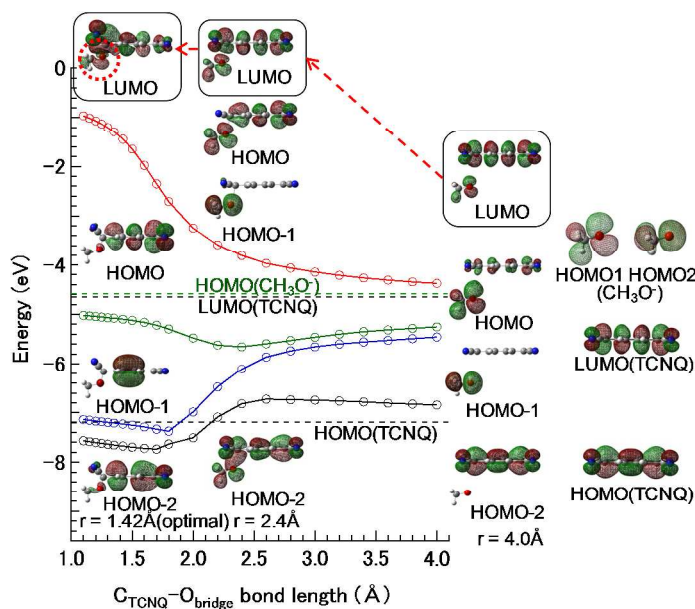CPCM is one of successful solvation models.[26] All the calculations were performed by using a Gaussian 09 software[27].

Fig. 4. Energies and electronic distributions (|isovalue| = 0.02) of HOMO-2 (black circles), HOMO-1 (blue circles), HOMO (green circles), and LUMO (red circles) in CH_3O-TCNQ$^-$ as a function of the C_{TCNQ}-O_{bridge} bond length. Gray: carbon, white: hydrogen, and red: oxygen atom. Green and brown isosurfaces stand for opposite signs in amplitude.

Results and discussion

Methoxy-TCNQ complex

At first, we examined a simple methoxy-TCNQ complex produced by a nucleophilic addition reaction between a methoxy anion and TCNQ, as shown in Fig. 3(a). Fig. 3(b) shows the calculated potential curve and structural change of the CH_3O-TCNQ$^-$ nucleophilic adduct as a function of the C_{TCNQ}-O_{bridge} bond length. The potential curve is concave downward with a binding energy of 1.84 eV, indicating its barrier-less exothermic reaction. As the nucleophilic addition reaction proceeds, the conformation of the attacked carbon atom (C_7 in Fig. 1) is changed from a planar to a tetragonal structure with the sp^2-to-sp^3 hybrid-orbital change. The C_{TCNQ}-O_{bridge} bond length in the minimum point was calculated to be 1.42 Å. This value is very close to the reported value (1.41 Å) determined by X-ray diffraction analysis[28]. This result indicates the validity of the DFT calculation.

Fig. 4 shows the energies and electronic distributions of the highest, second highest and third highest molecular orbitals (HOMO, HOMO-1 and HOMO-2, respectively) and lowest unoccupied molecular orbital (LUMO) of CH_3O-TCNQ$^-$. Before the nucleophilic addition, the LUMO of TCNQ is located slightly below the two degenerate HOMOs (HOMO1, HOMO2) of a methoxy anion and, on the other hand, the HOMO of TCNQ exists much below the HOMO1 and HOMO2. Because of the energetic proximity and orbital symmetry in overlap integral, the LUMO of TCNQ strongly
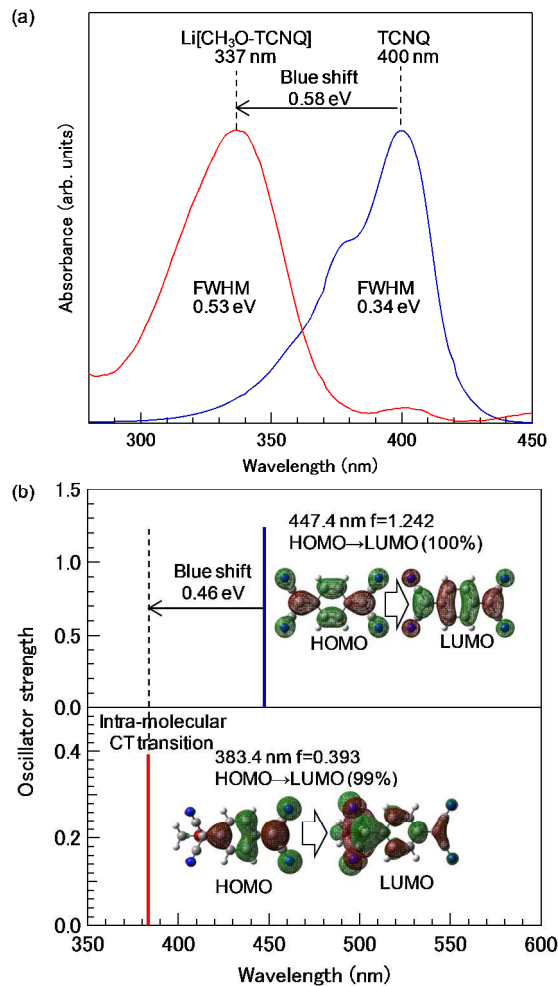
interacts with the HOMO1 of the methoxy anion. Consequently, the LUMO energy of TCNQ significantly increases from -4.64 to -1.44 eV

Fig. 5. (a) Experimental absorption spectra of TCNQ (blue) and CH_3O-TCNQ$^-$ (red) in chloroform and (b) calculated electronic excitation spectra of TCNQ (blue) and CH_3O-TCNQ$^-$ (red). Green and brown isosurfaces (|isovalue| = 0.02) stand for opposite signs in amplitude.

by the anti-bonding interaction with the HOMO1, as shown by a red dashed circle. This result indicates that the electron-accepting property of TCNQ vanishes at all by the nucleophilic addition reaction with a methoxy anion and CH_3O-TCNQ$^-$ has a rather electron-donating property. In addition to the significant elevation, the electronic distribution of the LUMO is moved toward the reaction site with remarkable delocalization on the attacking oxygen atom, as shown by the red dashed circle in Fig. 4. The considerable elevation and electronic redistribution of the LUMO are favorable for strong coupling with the d orbitals of a surface Ti atom on TiO_2, as will be described later. On the other hand, the HOMO of CH_3O-TCNQ$^-$ has almost no distribution on the oxygen atom and the increase in the energy is moderate. As a result, the HOMO-LUMO gap energy increases from 2.55 eV to 3.66 eV by the nucleophilic addition reaction.

In order to confirm the calculation results in Fig. 4, we calculated electronic excitation spectra of TCNQ and CH$_3$O-TCNQ$^-$ and compared with the reported experimental
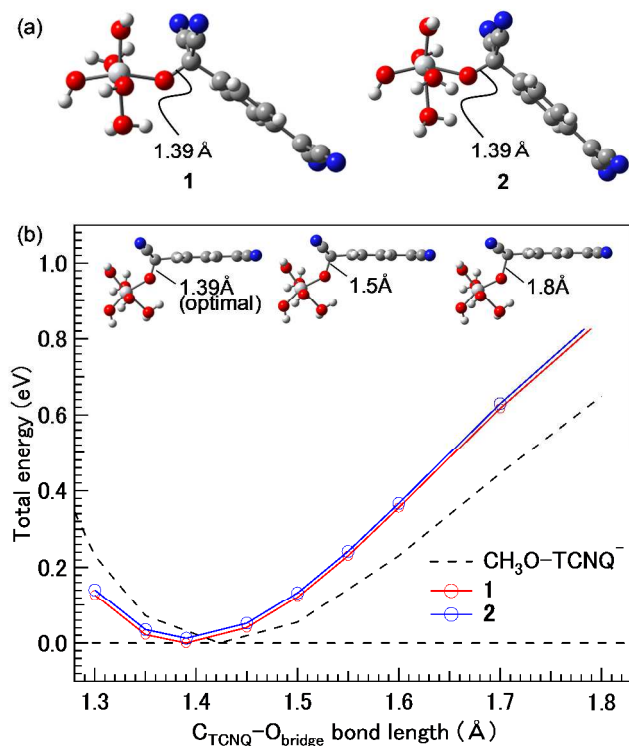

Fig. 6. (a) Optimized structures of model compounds **1** and **2** and (b) calculated potential curves of **1** (red) and **2** (blue) along the reaction coordinate together with that of CH$_3$O-TCNQ-. The minimum energy of CH$_3$O-TCNQ- is set to that of **1**. Large gray: titanium, small gray: carbon, white: hydrogen, and red: oxygen atom.

absorption spectra[28]. Fig. 5(a) shows experimental absorption spectra[29] of TCNQ and CH$_3$O-TCNQ$^-$. TCNQ shows an absorption band at 400 nm with a vibration structure (vibrational energy: ca. 0.172 eV). On the other hand, CH$_3$O-TCNQ$^-$ shows an absorption band at 337 nm without any vibration structure.[28] As compared to the absorption band of TCNQ, the absorption band of CH$_3$O-TCNQ$^-$ is blue-shifted by 0.58 eV. In addition, the absorption band is slightly broader than that of TCNQ. The full width at a half maximum (FWHM) of the absorption band in CH$_3$O-TCNQ$^-$ was estimated to be 0.53 eV, which is larger than that (0.34 eV) for TCNQ. Fig. 5(b) shows calculated electronic excitation spectra of TCNQ and CH$_3$O-TCNQ$^-$.[30] The wavelength of the lowest singlet electronic excitation in TCNQ was estimated as 447.4 nm and the one in CH$_3$O-TCNQ$^-$ as 383.4 nm. Although these calculated excitation wavelengths are overestimated as compared to the experimental data, the blue shift of the absorption band is reproduced by the TD-DFT calculations. The calculated amount (0.46 eV) of the blue shift is comparable to the experimental value (0.58 eV). Both the absorption bands in TCNQ and CH$_3$O-TCNQ$^-$ are attributed to the HOMO→LUMO transition. Therefore, the blue-shift is consistent with the widening of the HOMO-LUMO gap by the

larger elevation of the LUMO of CH$_3$O-TCNQ$^-$. In addition, the broadening and vanishing of the vibrational structure are supported by the intra-molecular charge-transfer nature of the
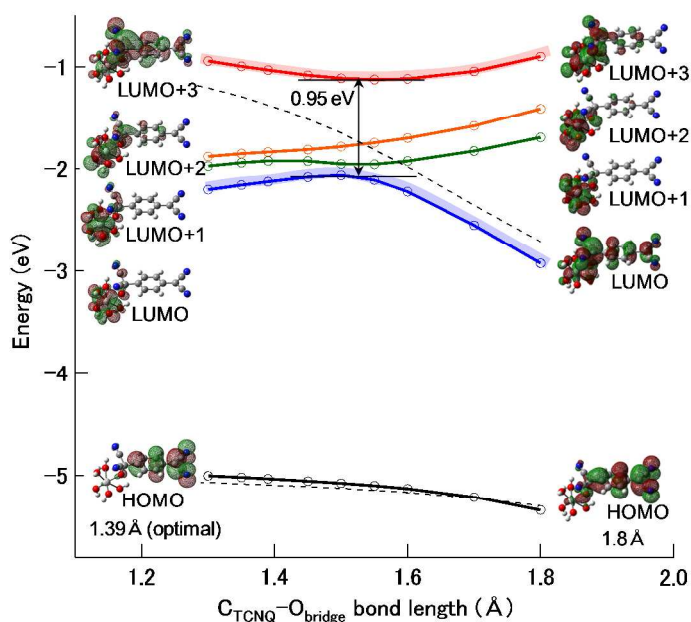

Fig. 7. Energies and electronic distributions ((|isovalue|=0.02)) of HOMO (black circles), LUMO (blue circles), LUMO+1 (green circles), LUMO+2 (orange circles), and LUMO+3 (red circles) in **1** together with those (black dashed curves) of HOMO and LUMO of CH$_3$O-TCNQ$^-$.

HOMO→LUMO transition in CH$_3$O-TCNQ$^-$, as shown in the inset of Fig. 5(b). The analyses of the electronic excitation spectra support the validity of the calculation results in Fig. 4.

TiO$_2$-TCNQ model complex

Fig. 6(a) shows two model complexes **1** and **2** (Ti(OH)$_3$(H$_2$O)$_2$(μ-O)TCNQ]$^-$) for the TiO$_2$-TCNQ surface complex (Fig. 1). Several mono-Ti model complexes with hydroxy groups at different positions were examined. **1** and **2** were found to be the most stable among the complexes. The C$_{TCNQ}$-O$_{bridge}$ bond length in the optimized structures of **1** and **2** was calculated to be 1.39 Å, which is slightly shorter than that (1.42 Å) of CH$_3$O-TCNQ$^-$. Fig. 6(b) shows the calculated potential curves of **1** and **2** along the reaction coordinate together with that of CH$_3$O-TCNQ$^-$. The minimum energy in CH$_3$O-TCNQ$^-$ was set to that in **1** for visualization purposes. The potential curves of **1** and **2** are very analogous with that of CH$_3$O-TCNQ$^-$. These results indicate that the binding energy is dominantly governed by the electron-donating property of the attacking oxygen atom and the electron-donating property of the attacking oxygen atom in **1** and **2** is comparable or slightly larger than that in CH$_3$O-TCNQ$^-$. As the reaction proceeds, the conformation of the attacked carbon atom of TCNQ is varied from a planar (sp^2) to a tetragonal (sp^3) similarly to the case of CH$_3$O-TCNQ$^-$. Since the structural and electronic properties of

2 are almost the same as those of **1**, hereafter results of **1** are mainly described.

Fig. 7 shows the energies and electronic distributions of the HOMO, LUMO, the second, third, and fourth lowest unoccupied molecular orbitals (LUMO+1, LUMO+2, and

Table 1. Electronic distributions (|isovalue|=0.05) of the HOMO, LUMO, LUMO+1, LUMO+2, and LUMO+3 at different C_{TCNQ}-O_{bridge} bond lengths (r) in **1**. D: delocalization on TCNQ and Ti, L(Ti): localization on Ti, L(TCNQ): localization on TCNQ.

r(Å)	H	L	L+1	L+2	L+3
1.3	L(TCNQ)	L(Ti)	L(Ti)	L(Ti)	D
1.39	L(TCNQ)	L(Ti)	L(Ti)	L(Ti)	D
1.5	L(TCNQ)	L(Ti)	L(Ti)	L(Ti)	D
1.6	L(TCNQ)	D	L(Ti)	L(Ti)	D
1.7	L(TCNQ)	D	L(Ti)	L(Ti)	L(Ti)
1.8	L(TCNQ)	D	L(Ti)	L(Ti)	L(Ti)

LUMO+3, respectively) in **1**.[31] In the figure, the HOMO and LUMO of CH_3O-$TCNQ^-$ are also shown by black dashed curves for comparison. At the C_{TCNQ}-O_{bridge} bond length of 1.8 Å, the HOMO and LUMO in **1** correspond to the HOMO and LUMO in CH_3O-$TCNQ^-$. On the other hand, the LUMO+1, LUMO+2, and LUMO+3 correspond to the $d(t_{2g})$ orbitals of the titanium atom, although the LUMO+3 is strikingly delocalized on the TCNQ moiety. As the nucleophilic addition reaction proceeds, the energy of the LUMO of **1** significantly increases in contrast to the HOMO. The changes of the HOMO and LUMO energies in **1** well agree with those in CH_3O-$TCNQ^-$. This result means that the striking elevation of the LUMO level in **1** is predominantly caused by the nucleophilic attack of the negatively charged oxygen atom. On the other hand, the energies of the LUMO+1, LUMO+2, and LUMO+3 gradually decrease. At the C_{TCNQ}-O_{bridge} bond lengths around 1.6 Å, an avoided crossing occurs between the LUMO and LUMO+1, LUMO+2 and LUMO+3, which clearly indicates the occurrence of electronic coupling between the π^* of the TCNQ moiety and $d(t_{2g})$ orbitals of the titanium atom. Table 1 shows the electronic distributions of the orbitals at the different C_{TCNQ}-O_{bridge} bond lengths. The isovalue was set to be 0.05 larger than

that in Fig. 7 in order to see the main distribution. The orbitals are divided into three classes. L(TCNQ) is localized on the TCNQ moiety, L(Ti) is localized on the titanium atom, and D is delocalized on TCNQ and the titanium atom. As shown in Table 1, the HOMO is localized on the TCNQ moiety at the all
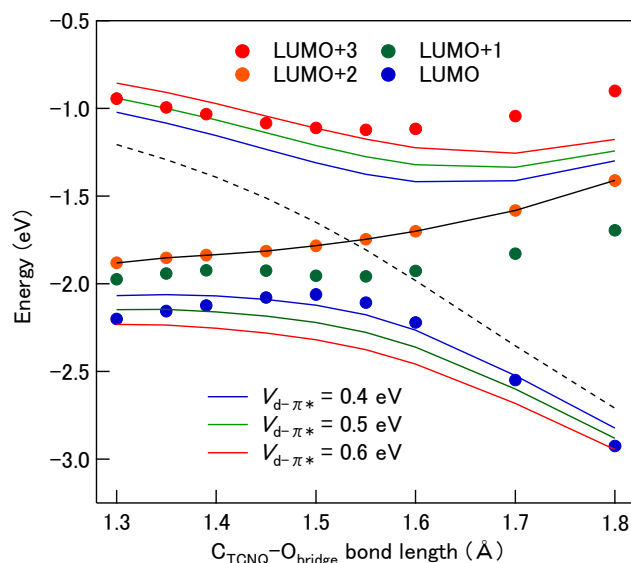

Fig. 8. Two-level system analysis of avoided crossing between the LUMO and LUMO+3 in **1** and simulated curves obtained from Eqs 2 and 3 with different $V_{d\text{-}\pi^*}$ values of 0.4 eV (blue curves), 0.5 eV (green curves), and 0.6 eV (red curves).

bond lengths. The LUMO+1 and LUMO+2 are predominantly localized on the Ti moiety at the all bond lengths. Note that the LUMO+1 and LUMO+2 in **1** are partially distributed on the dicyanomethylene group, as shown with the smaller isovalue in Fig. 7. On the other hand, the LUMO at the C_{TCNQ}-O_{bridge} bond lengths of 1.6-1.8 Å and LUMO+3 at 1.3-1.6 Å are classified into D, showing the strong d-π^* interaction. The splitting energy of the avoided crossing between the LUMO and LUMO+3 was estimated to be ca. 0.95 eV, as shown in Fig. 7.

The avoided crossing between the LUMO and LUMO+3 due to the d-π^* interaction was analyzed in a two-level system in order to quantitatively evaluate the coupling energy. The Hamiltonian matrix in the $|d\rangle$ and $|\pi^*\rangle$ systems is expressed as follows.

$$H_{d\text{-}\pi^*}(r) = \begin{pmatrix} E_d(r) & V_{d-\pi^*}(r) \\ V_{d-\pi^*}(r) & E_{\pi^*}(r) \end{pmatrix} \quad (1)$$

The diagonal and off-diagonal elements are dependent on the C_{TCNQ}-O_{bridge} bond length (r). The eigenvalues (E_1 and E_2) are obtained by diagonalization of the Hamiltonian matrix as follows.

$$E_1(r) = \frac{E_d(r) + E_{\pi^*}(r)}{2} - \sqrt{\left(\frac{E_d(r) - E_{\pi^*}(r)}{2}\right)^2 + V_{d-\pi^*}(r)^2} \quad (2)$$

$$E_2(r) = \frac{E_d(r) + E_{\pi^*}(r)}{2} + \sqrt{\left(\frac{E_d(r) - E_{\pi^*}(r)}{2}\right)^2 + V_{d-\pi^*}(r)^2} \quad (3)$$

Strictly speaking, it is very difficult to explicitly determine the $E_d(r)$ and $E_{\pi*}(r)$ functions. However, the $E_d(r)$ function is considered to be analogous to that of the LUMO+2 in **1** that has little distribution on the TCNQ moiety. The $E_{\pi*}(r)$ function
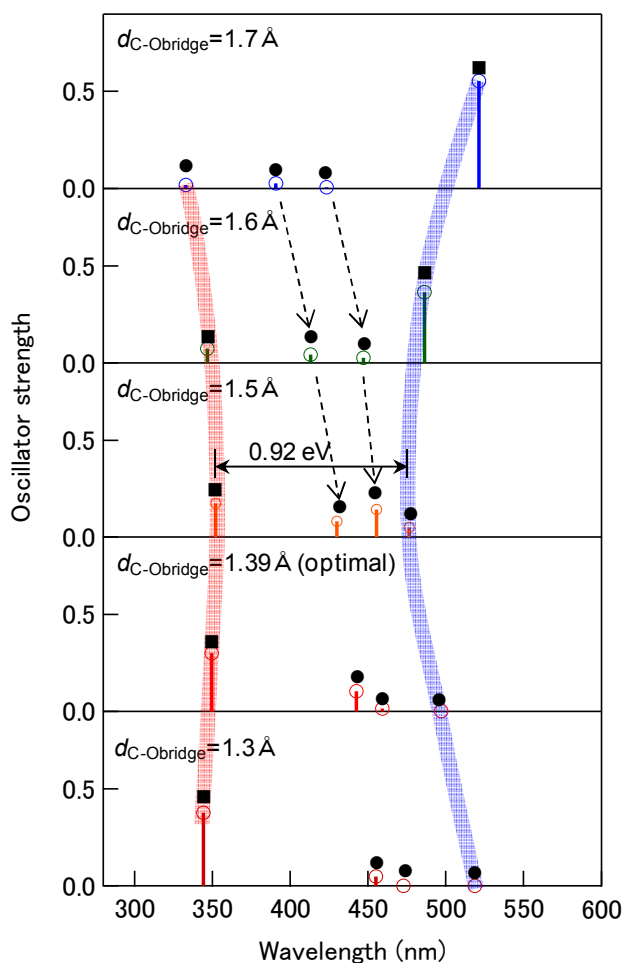

Fig. 9. Calculated electronic excitation spectra at different C_{TCNQ}-O_{bridge} bond lengths in **1**. Solid circles and squares stand for complete and partial ICT transitions, respectively.
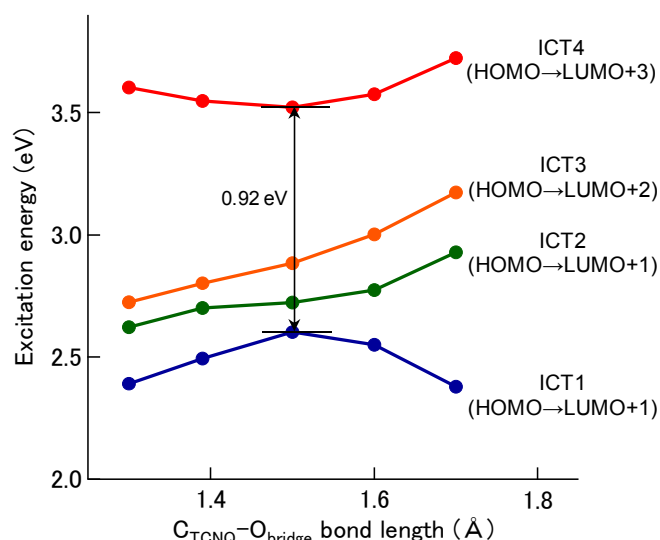

Fig. 10. Excitation energies of complete and partial ICT transitions in **1** as a function of the C_{TCNQ}-O_{bridge} bond length.

would be very similar to that of the LUMO of CH_3O-$TCNQ^-$, since the HOMO behaviour of **1** is in good agreement with that of CH_3O-$TCNQ^-$, as shown in Fig. 7. For this reason, tentatively assuming that $E_d(r)$ and $E_{\pi*}(r)$ behave likewise the LUMO+2 in **1** and the LUMO of CH_3O-$TCNQ^-$, respectively, $E_1(r)$ and $E_2(r)$ were calculated, as shown in Fig. 8. Despite the rough assumption, the avoided crossing is well reproduced with the coupling energy ($V_{d-\pi*}$) of ca. 0.5 eV.

Next, we examined the question of how the d-$\pi*$ interaction enhances the ICT-transition probabilities. Fig. 9 shows calculated electronic excitation spectra of **1** at different C_{TCNQ}-O_{bridge} bond lengths. Excitation wavelengths, oscillator strengths, contributions, and excitation characters are tabulated in Table 2. In the near UV and visible regions, four electronic transitions from the HOMO to the LUMO, LUMO+1,

Table 2. Excitation wavelengths, oscillator strengths, main configurations, and excitation properties at different C_{TCNQ}-O_{bridge} bond lengths in **1**.

| C_{TCNQ}-O_{bridge} bond length (Å)	Excitation wavelength (nm)	Oscillator strength	Main configuration	Character
1.3	518.7	0.0001	HOMO→LUMO(100%)	Complete ICT
	472.8	0.0003	HOMO→LUMO+1(100%)	Complete ICT
	455.2	0.0491	HOMO→LUMO+2(100%)	Complete ICT
	344.2	0.3770	HOMO→LUMO+3(97%)	Partial ICT
1.39 (optimal)	497.2	0.0020	HOMO→LUMO(100%)	Complete ICT
	459.2	0.0144	HOMO→LUMO+1(99%)	Complete ICT
	442.6	0.1040	HOMO→LUMO+2(99%)	Complete ICT
	349.6	0.3006	HOMO→LUMO+3(98%)	Partial ICT
1.5	476.6	0.0500	HOMO→LUMO(98%)	Complete ICT
	455.5	0.1424	HOMO→LUMO+1(98%)	Complete ICT
	430.0	0.0809	HOMO→LUMO+2(99%)	Complete ICT
	352.2	0.1736	HOMO→LUMO+3(98%)	Partial ICT
1.6	486.3	0.3651	HOMO→LUMO(99%)	Partial ICT
	447.1	0.0253	HOMO→LUMO+1(99%)	Complete ICT
	413.2	0.0423	HOMO→LUMO+2(99%)	Complete ICT
	346.8	0.0732	HOMO→LUMO+3(98%)	Partial ICT
1.7	521.2	0.5543	HOMO→LUMO(100%)	Partial ICT
	423.4	0.0048	HOMO→LUMO+1(99%)	Complete ICT
	390.8	0.0265	HOMO→LUMO+2(99%)	Complete ICT
	333.1	0.0177	HOMO→LUMO+3(93%)	Complete ICT
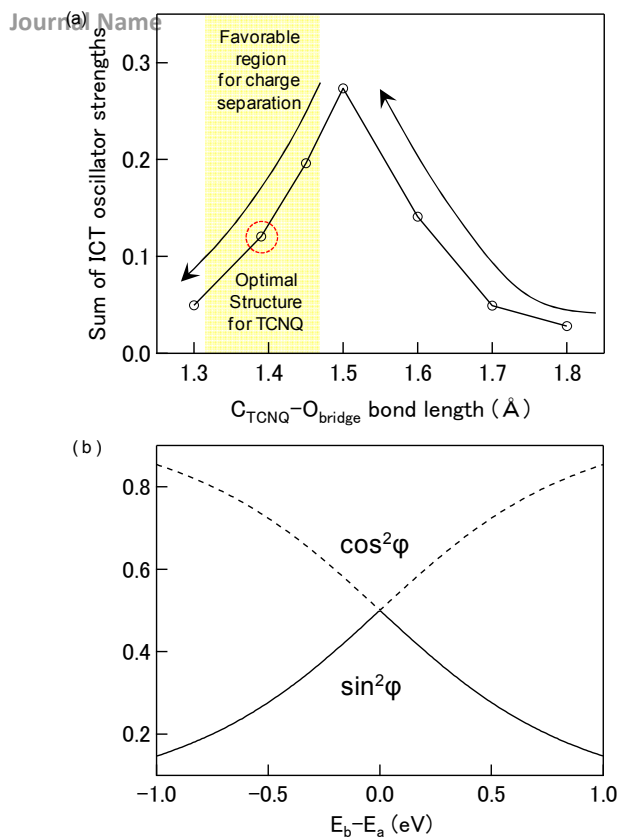
Fig. 11. (a) Sum of oscillator strengths of complete ICT transitions in **1** as a function of the C_{TCNQ}-O_{bridge} bond length and (b) $sin^2\varphi$ and $cos^2\varphi$ in a two-level system with an off-diagonal element of 0.5 eV as a function of the energy difference ($E_2 - E_1$). See text for detail.

LUMO+2, and LUMO+3 occur. Those four transitions are classified into the complete ICT transition and partial ICT transition from the molecular-orbital characters in Table 1. For the complete ICT transition, the unoccupied orbital is predominantly localized on the titanium atom. Thus, an electron is entirely injected into the titanium atom. On the other hand, for the partial ICT transition, the unoccupied orbital is delocalized on TCNQ and the titanium atom, resulting in partial electron injection in TiO_2. In the optimal structure, complete ICT transitions occur in the visible region and the intra-molecular CT excitation at 350 nm in the near UV region. This result is consistent with the assignment of the broad absorption band in Fig. 2(a) to the complete ICT transitions.[7,14-17] In addition, an avoided crossing is discernible in the excitation spectra, as shown by red and blue curves in Fig. 9. The avoided crossing in the excited states is more clearly manifested in Fig. 10. The splitting energy between the ICT1 and ICT4 excitations was estimated to be ca. 0.92 eV that is comparable to that of the avoided crossing between the LUMO and LUMO+3 in Fig. 7. Since the lowest and forth lowest excitations (ICT1 and ICT4) are attributed to the HOMO→LUMO and HOMO→LUMO+3 transitions, respectively, as shown in Table 2, it is reasonable that the splitting energy between the ICT1 and ICT4 is almost equal to that between the LUMO and LUMO+3. Thus, the excited-state coupling originates from the d-π^* electronic interaction (ca. 0.5 eV). Note that although the large splitting between the ICT1 and ICT4 is highlighted above, excited-state

couplings of the ICT1 with the ICT2 and ICT3 also occur, because the oscillator strengths of the ICT2 and ICT3 are strikingly enhanced. Taking into account this fact, the sum of the oscillator strengths of the complete ICT excitations were calculated as a function of the C_{TCNQ}-O_{bridge} bond length, as shown in Fig. 11(a). With decreasing the bond length, the value rapidly increases with a maximum at 1.5 Å and, then, decreases. The value at 1.39 Å (optimal) is about 44% of the maximum value. This result evidently reveals that the ICT transitions are enhanced by the coupling with the intra-molecular CT excitation due to the strong d-π^* electronic interaction (ca. 0.5 eV).

In order to understand the above-mentioned bond-length dependence qualitatively, it is useful to employ a two-level system. Considering two excited states of |a> and |b>, the Hamiltonian matrix is described as follows within a framework of a two-level system.

$$H_{a,b}(r) = \begin{pmatrix} E_a(r) & V_{a,b}(r) \\ V_{a,b}(r) & E_b(r) \end{pmatrix} \quad (4)$$

The eigenenergies are given by similar equations to Eqs 2and 3. The coupling energy ($V_{a,b}(r)$) is reasonably considered to be almost the same as $V_{d-\pi^*}(r)$. The eigenfunctions (|i> and |ii>) are described by the following equations.

$$|i\rangle = cos\varphi|a\rangle + sin\varphi|b\rangle \quad (5)$$

$$|ii\rangle = -sin\varphi|a\rangle + cos\varphi|b\rangle \quad (6)$$

$$sin^2\varphi = \frac{1}{2}\left[1 - \left\{1 + \left(\frac{2V_{a,b}(r)}{E_a(r)-E_b(r)}\right)^2\right\}^{-\frac{1}{2}}\right] \quad (7)$$

$$cos^2\varphi = \frac{1}{2}\left[1 + \left\{1 + \left(\frac{2V_{a,b}(r)}{E_a(r)-E_b(r)}\right)^2\right\}^{-\frac{1}{2}}\right] \quad (8)$$

The coefficient of the coupling of the complete ICT transition with the partial ICT transition is described as $sin\varphi$. Supposing that |a> and |b> are the complete and partial ICT excitations, respectively, the transition probability from the ground state |g> to the excited state |i> is described as follows.

$$P \propto |cos\varphi\langle a|e\boldsymbol{r}|g\rangle + sin\varphi\langle b|e\boldsymbol{r}|g\rangle|^2 \quad (9)$$

Fig. 11(b) shows $cos^2\varphi$ and $sin^2\varphi$ as a function of the energy difference ($E_b(r) - E_a(r)$) with $V_{a,b}(r)$ of 0.5 eV. $cos^2\varphi$ increases with the absolute value of the energy difference. On the other hand, $sin^2\varphi$ decreases with increasing the absolute value of the energy difference. The behavior of $sin^2\varphi$ is in good agreement with the bond-length dependence in Fig. 11(a). This result is reasonable from the fact that the transition probability of the complete ICT transition is approximated by the following equation since the probability of the complete ICT transition is

much lower than that of the partial ICT transition, as shown in Fig. 9.

$$P \propto sin^2\varphi\langle b|e\boldsymbol{r}|g\rangle^2 \quad (10)$$

Therefore, the mechanism of the enhancement of the ICT transitions in the TiO$_2$-TCNQ hybrid material was clarified.

For applications of ICT transitions as a charge separation mechanism for solar energy conversions, the energy of the partial ICT excitation should be larger than that of the complete ICT excitation, otherwise electrons injected in TiO$_2$ by the complete ICT transitions return to TiO$_2$ surfaces, which suffers from carrier recombination. For this reason, a yellow region in Fig. 11(a) is favorable for applications to solar energy conversions, keeping the strong ICT transitions. In fact, the TiO$_2$-TCNQ exists within the area.

Finally, we discuss the validity and difference of the mono-Ti model compound with the experimentally used TiO$_2$ nanoparticle-TCNQ hybrid material. At first, the calculated LUMO energy (-2.12 eV) of the mono-Ti model complex is much higher than the energy (ca. -4.0 eV) of the conduction-band bottom of TiO$_2$, as shown in Fig. 7. The higher energy of the LUMO level is attributed not only to the lack of the stabilization due to bonding interactions with other titanium and oxygen atoms, but also to the total negative charge. In addition, the unoccupied orbitals of the mono-Ti model compound are localized on the titanium atom, as shown in Fig. 7. On the other hand, the unoccupied orbitals on TiO$_2$ surfaces are considered to be delocalized on the TiO$_2$ moiety to some extent.[14,16] The delocalization likely decreases the organic-inorganic electronic coupling energy. In order to get a more quantitative insight, analyses with TiO$_2$ nanoclusters are crucial. However, as mentioned in Introduction, surface structures of TiO$_2$ nanoparticles have not yet been understood well. For example, the question of how crystalline or how amorphous TiO$_2$ surface are still remains to be studied. For this reason, the use of the mono-Ti model complex would be appropriate. Indeed, the ICT-transition nature and excitation energies are well reproduced by the DFT and TD-DFT calculations. From this viewpoint, this work based on the mono-Ti model complex provides important knowledge on the mechanisms of the organic-inorganic electronic coupling and the enhancement of the ICT transitions in the TiO$_2$-TCNQ hybrid material as a first step.

Conclusion

In this work, we studied the strong organic-metal oxide semiconductor electronic coupling caused by the surface nucleophilic addition reaction in the TiO$_2$-TCNQ hybrid material. The mechanisms of the strong electronic coupling and the enhancement of the ICT-transition probability were clarified in detail. The coupling energy was estimated to be ca. 0.5 eV based on the DFT analysis with the mono-Ti model

compound. To our best knowledge, such strong coupling at organic-inorganic interfaces was first demonstrated.

Acknowledgements

Notes and references

[a]Graduate School of Science and Technology, Gunma University, 1-5-1 Tenjin-cho, Kiryu, Gunma, 376-8515, Japan. E-mail: jfujisawa@gunma-u.ac.jp
[b]Japan Science and Technology Agency (JST), Precursory Research for Embryonic Science and Technology (PRESTO), 4-1-8 Honcho Kawaguchi, Saitama 332-0012, Japan.

1 K. Kalyanasundaram, *Dye-Sensitized Solar Cells*, EPFL Press, 2010.
2 T. Horiuchi, J. Fujisawa, S. Uchida and M. Grätzel, *Data Book on Dye-Sensitized Solar Cells*, CMC Publishing Co., Tokyo, 2009.
3 H. Kisch, *Semiconductor Photocatalysis: Principles and Applications*, Wiley-VCH, 2014.
4 J. Moser, S. Punchihewa, P. P. Infelta and M. Grätzel, *Langmuir*, 1991, **7**, 3012.
5 R. Rodriguez, M. A. Blesa and A. E. Regazzoni, *J. Colloid Interf. Sci.*, 1996, **177**, 122.
6 Y. S. Seo, C. Lee, K. H. Lee and K. B. Yoon, *Angew. Chem. Int. Ed.*, 2005, **44**, 910.
7 T. Kubo, J. Fujisawa and H. Segawa, *Electrochemistry*, 2009, **77**, 977.
8 M. Bledowski, L. Wang, A. Ramakrishnan, O. V. Khavryuchenko, V. D. Khavryuchenko, P. C. Ricci, J. Strunk, T. Cremer, C. Kolbeckf and R. Beranek, *Phys. Chem. Chem. Phys.*, 2011, **13**, 21511.
9 J. Fujisawa and M. Nagata, *Chem. Phys. Lett.*, 2015, **619**, 180.
10 J. Fujisawa and T. Ishihara, *Phys. Rev. B*, 2004, **70**, 113203.
11 J. Fujisawa and N. Tajima, *Phys. Rev. B*, 2005, **72**, 125201.
12 J. Fujisawa, N. Tajima, K. Tamaki, M. Shimomura and T. Ishihara, *J. Phys. Chem. C*, 2007, **111**, 1146.
13 J. Fujisawa and G. Giacomo, *Phys. Chem. Phys. Chem.*, 2014, **16**, 17955.
14 R. Jono, J. Fujisawa, H. Segawa and K. Yamashita, *J. Phys. Chem. Letters*, 2011, 2, 1167.
15 S. Manzhos, R. Jono, K. Yamashita, J. Fujisawa, M. Nagata and H. Segawa, *J. Phys. Chem. C*, 2011, **115**, 21487.
16 R. Jono, J. Fujisawa, H. Segawa and K. Yamashita, *Phys. Chem. Chem. Phys.*, 2013, **15**, 18584.
17 J. Fujisawa, *Phys. Chem. Chem. Phys.*, 2015, **17**, 12228.
18 Kohn W and Sham, *Phys. Rev.*, 1965, **140**, A1133.
19 A.D. Becke, *J. Chem. Phys.*, 1993, **98**, 5648.
20 C. Lee, W. Yang and R. G. Parr, *Phys. Rev. B*, 1988, **37**, 785.
21 R. Ditchfield, W. Hehre and J. Pople, *J. Chem. Phys.*, 1971, **54**, 724.
22 W. Hehre, R. Ditchfield and J. Pople, *J. Chem. Phys.*, 1972, **56**, 2257.
23 M. A. L. Marques and E. K. U. Gross. *Annu. Rev. Phys. Chem.*, 2004, **55**, 427.
24 V. Barone and M. Cossi, *J. Phys. Chem. A*, 1998, **102**, 1995.

25 M. Cossi, N. Rega, G. Scalmani and V. Barone, *J. Comput. Chem.*, 2003, **24**, 669.

26 Y. Takano and K. N. Houk, *J. Chem. Theory Comput.*, 2005, **1**, 70.

27 M. J. Frisch *et al*. Gaussian 09, revision D.01; Gaussian, Inc.: Wallingford, CT, 2009.

28 T. Murata, G. Saito, K. Nishimura, Y. Enomoto, G. Honda, Y. Shimizu, S. Matsui, M. Sakata, O. O. Drozdova and K. Yakushi, *Bull. Chem. Soc. Jpn.*, 2008, **81**, 331.

29 J. Fujisawa and T. Nagatani, Unpublished results.

30 Structural optimization and electronic excitation spectra of TCNQ and $CH_3O\text{-}TCNQ^-$ were calculated taking into account solvation effects of chloroform that was used as solvent in the experiment in Fig. 5(a). The excitation wavelength was calculated to be 454.5 nm for TCNQ and 403.2 nm for $CH_3O\text{-}TCNQ^-$. Although the excitation wavelengths are overestimated in the TD-DFT calculations as compared to the experimentally observed absorption wavelengths (400 nm for TCNQ and 337 nm for $CH_3O\text{-}TCNQ^-$), the blue-shift in $CH_3O\text{-}TCNQ^-$ is reproduced. Qualitative difference in the calculation result between acetonitrile and chloroform is not seen.

31 Unfortunately, structural optimization at the $C_{TCNQ}\text{-}O_{bridge}$ bond lengths longer than 1.8 Å was not converged for **1** and **2**.